TITLE:

CD5 levels reveal distinct basal T cell receptor signals in T cells from non-obese diabetic mice

RUNNING TITLE

Distinct basal TCR signals in NOD mice

AUTHORS:

Mengqi Dong[1, 2], Cindy Audiger[1, 2], Adeolu Adegoke[3], Marie-Ève Lebel[1, 2], Stefanie F. Valbon[1, 2], Colin C. Anderson[4], Heather J. Melichar[1, 5], Sylvie Lesage[1, 2]

AFFILIATIONS:

1. Immunology-Oncology Unit, Maisonneuve-Rosemont Hospital Research Center, Montréal, Québec, H1T 2M4, Canada
2. Département de microbiologie, infectiologie et immunologie, Université de Montréal, Montréal, Québec, H3T 1J4, Canada
3. Departments of Surgery, Alberta Diabetes Institute, University of Alberta, Edmonton, Alberta, T6G 2R3, Canada.
4. Departments of Surgery and Medical Microbiology & Immunology, Alberta Diabetes Institute, Alberta Transplant Institute, University of Alberta, Edmonton, Alberta, T6G 2R3, Canada.
5. Département de médecine, Université de Montréal, Montréal, Québec, H3T 1J4, Canada

Address correspondence to: Heather J. Melichar (heather.melichar@umontreal.ca) or Sylvie Lesage (sylvie.lesage@umontreal.ca)

Abstract

Type 1 diabetes in non-obese diabetic (NOD) mice occurs when autoreactive T cells eliminate insulin producing pancreatic β cells. While extensively studied in T cell receptor (TCR) transgenic mice, the contribution of alterations in thymic selection to the polyclonal T cell pool in NOD mice is not yet resolved. The magnitude of signals downstream of TCR engagement with self-peptide directs the development of a functional T cell pool, in part by ensuring tolerance to self. TCR interactions with self-peptide are also necessary for T cell homeostasis in the peripheral lymphoid organs. To identify differences in TCR signal strength that accompany thymic selection and peripheral T cell maintenance, we compared CD5 levels, a marker of basal TCR signal strength, on immature and mature T cells from autoimmune diabetes-prone NOD and -resistant B6 mice. The data suggest that there is no preferential selection of NOD thymocytes that perceive stronger TCR signals from self-peptide engagement. Instead, NOD mice have an MHC-dependent increase in $CD4^+$ thymocytes and mature T cells that express lower levels of CD5. In contrast, T cell-intrinsic mechanisms lead to higher levels of CD5 on peripheral $CD8^+$ T cells from NOD relative to B6 mice, suggesting that peripheral $CD8^+$ T cells with higher basal TCR signals may have survival advantages in NOD mice. These differences in the T cell pool in NOD mice may contribute to the development or progression of autoimmune diabetes.

Keywords

thymic selection, NOD, B6.*H2*^{g7}, CD5, TCR signals

Introduction

T cell differentiation proceeds in the thymus, where central tolerance mechanisms allow for the production of a functional, self-tolerant pool of T cells bearing antigen receptors with low to moderate affinity for self-peptide major histocompatibility complex (MHC) complexes [1]. Deletional mechanisms mediate negative selection of many thymocytes expressing T cell receptors (TCR) that are overtly reactive to ubiquitous or tissue-specific self-antigens, such as insulin. Additionally, some thymocytes with relatively high reactivity to self-peptide can be diverted to immunomodulatory lineages or become anergic [2-5]. The effectiveness of central tolerance mechanisms is thus highly dependent on the ability of thymocytes to perceive the strength of the TCR interaction with self-peptide MHC complexes [1, 6]. Defects in these processes can lead to an increased production of potentially autoreactive T cells and contribute to autoimmune susceptibility [7].

Non-obese diabetic (NOD) mice spontaneously develop autoimmune diabetes [8, 9]. In this model, autoreactive T cells in the periphery are necessary and sufficient for mediating the destruction of insulin-producing β cells in the pancreas, leading to disease onset [8, 9]. As such, it has been proposed that defects in central tolerance in NOD mice result in the 'escape' of functional, high affinity autoreactive T cells from the thymus, increasing autoimmune susceptibility. While the sensitivity of NOD thymocytes to apoptosis following anti-CD3 stimulation is debatable [10, 11], the use of various TCR transgenic models demonstrate that thymic selection processes are altered in mice on the NOD genetic background as compared to autoimmune resistant strains [12-19]. However, it is not clear whether alterations in thymic selection permit the differentiation and thymic exit of high affinity autoreactive T cells in non-TCR transgenic NOD mice.

Here we revisit thymocyte selection of polyclonal T cells in NOD mice. Thymocyte fate is dependent on the perceived strength of TCR interactions with self-peptide MHC complexes [1]. The perceived strength of these interactions on T cell fate is dependent on many factors such as MHC, peptide, co-stimulatory molecules, type and abundance of antigen presenting cells, and molecular mediators of the TCR signalling cascade, among others [1, 2, 6]. NOD mice carry genetic polymorphisms that influence most, if not all, of these parameters [9, 20-25], which likely positively

or negatively impact the strength of thymocyte interactions with self-peptide or how thymocytes perceive these interactions. The overall strength of the TCR signal perceived by individual thymocytes can be quantified by cell surface expression of CD5 [26]. During thymic selection, CD5 levels are upregulated on developing T cells and are maintained on peripheral naïve T cells through continuous interactions between the TCR and self-peptide MHC [3, 26]. Generally, T cells with higher levels of CD5 express TCRs with stronger reactivity to self-peptide and stronger basal TCR signalling [27-30]. Therefore, variations in CD5 expression reflect the heterogeneity of individual T cells in their integration of TCR signals and can be used to quantify the perceived strength of TCR interactions with self-peptide MHC. By comparing CD5 levels on polyclonal immature and mature T cells harvested from autoimmune diabetes-prone NOD versus autoimmune-resistant B6 mice, we find that thymic selection in NOD mice is not inherently skewed to promote the differentiation of thymocytes with overtly high affinity for self-peptides, while peripheral $CD8^+$ T cells with higher affinity for self-peptide may have survival advantages on the NOD background.

Results

NOD mice do not generate thymocytes that perceive stronger TCR signals than those from B6 mice

The NOD MHC H-2^{g7} locus, encoding for class I K^{d} and D^{b} molecules and the unique class II I-A^{g7} molecule, is known to affect peptide presentation and likely influences the strength of TCR interactions with peptide MHC [31-33]. Therefore, to study how NOD thymocytes interpret TCR signal strength, we chose to include comparisons to B6 mice in addition to B6.*NOD-Idd1* mice which are congenic for the H-2^{g7} locus and hereafter referred to as B6^{g7} [34]. The H-2^{g7} locus in B6^{g7} mice encompasses the entire NOD MHC locus, encoding all MHC genes, as well as some non-MHC genes. Comparison of B6 and B6^{g7} allows us to decipher the impact of variations between the H-2^{b} and H-2^{g7} loci, while comparison of B6^{g7} to NOD will reveal the impact of non-MHC related factors on the development of the T cell pool. Importantly, T cell development is not overtly aberrant in NOD mice, as both the proportion and number of CD4^{+} and CD8^{+} single positive (SP) thymocytes and thymic Tregs (tTregs) are comparable between the B6 and NOD strains (Supplementary Figure 1). This is also in line with previous findings that suggest that young B6 and NOD mice have a similar number of peripheral T cells in the spleen [35, 36].

To determine how thymocytes interpret TCR interactions with self-peptide MHC, we compared CD5 levels on CD4^{+} and CD8^{+} SP thymocytes, as well as tTregs, from autoimmune diabetes-resistant B6 and B6^{g7} and diabetes-susceptible NOD mice. In the thymus, CD5 expression is typically lowest on CD8^{+} SP thymocytes, relatively higher on CD4^{+} SP thymocytes and highest on tTregs, in line with the strength of the TCR signal required to facilitate the differentiation of these respective T cell subsets [3, 26, 37, 38]. This trend is observed in all three mouse strains as evidenced by the relative fluorescence intensity (RFI) of CD5 on these subsets (Figure 1a,b and gating strategy in Supplementary Figure 1a). CD5 levels are similar on CD8^{+} SP thymocytes from all three strains (Figure 1a, b) suggesting that selection of thymocytes in NOD mice does not facilitate the differentiation of CD8^{+} SP thymocytes that perceive stronger TCR interactions with self-peptide MHC. Interestingly, we find that the mean of CD5 expression on CD4^{+} SP thymocytes from B6^{g7} and NOD mice is significantly lower than their B6 counterparts (Figure 1a,b). In addition, the coefficient of variation (CV) for CD5 expression, which reflects the breadth of expression of CD5, is significantly broader on the B6^{g7} and NOD CD4^{+} SP populations than on

those from B6 mice (Figure 1a, c). Therefore, the H-2^{g7} MHC locus, likely the I-A^{g7} molecule, favours positive selection of CD4$^+$ SP thymocytes with weaker, not stronger, TCR signals. For tTregs, which are also selected on MHC II, the relative expression of CD5 is surprisingly not different between B6, B6^{g7} and NOD mice (Figure 1a, b). Notably, while there are few mature CD4$^+$ and CD8$^+$ T cells that recirculate to the thymus, about half of the Tregs in the thymus are composed of those that have recirculated from the periphery in all three mouse strains (Supplementary Figure 2a-c, e-g) [39-41]. The relative expression of CD5 in CD4$^+$ and CD8$^+$ SP thymocytes was not affected by the exclusion of recirculating T cells (Supplementary Figure 2d, h). However, when recirculating Tregs are excluded from the analysis, the mean expression of CD5 parallels that of CD4$^+$ SP thymocytes, in that Tregs from both B6^{g7} and NOD mice have a lower level of CD5 expression relative to B6 mice (Figure 1d). Altogether, our results suggest that NOD mice do not have overt defects in clonal deletion as the upper threshold for positively selected T cells does not seem to differ between B6 and NOD mice and that the H-2^{g7} MHC locus allows positive selection of CD4$^+$ SP thymocytes and tTregs that perceive relatively weaker TCR signals.

In the periphery, the relative levels of CD5 expression are maintained on CD4$^+$ T cells and increased on NOD CD8$^+$ T cells

The relative expression levels of CD5 for each T cell subset, which are set during thymic positive selection, are generally maintained on naïve T cells in the periphery by the continuous interactions with self-peptide MHC that are required for their survival [27, 42]. Considering that TCR interactions with self-peptide MHC in the periphery are influenced by additional factors to those present in the thymus [43-45], we assessed whether the relative differences in CD5 levels on peripheral T cell subsets was maintained in all three strains. Indeed, we find that CD5 expression is lowest in naïve CD8$^+$ T cells, relatively higher on naïve CD4$^+$ T cells and highest on Tregs for all mouse strains (Figure 2a, b, and gating strategy in Supplementary Figure 3a). In addition, as observed in the thymus, naïve CD4$^+$ T cells and Tregs from B6^{g7} and NOD mice express lower levels of CD5, and the breadth of CD5 expression is greater than in B6 mice (Figure 2a-c). Also, in the pancreatic lymph nodes, CD5 levels on naïve CD8$^+$ T cells from all three strains are not significantly different (Figure 2a, b). However, CD5 levels are modestly increased on naïve CD8$^+$ T cells in peripheral lymph nodes from NOD mice (Figure 2a, b). Interestingly, the variations in CD5 expression on CD4$^+$ and CD8$^+$ T cells display similar trends in B6 and NOD mice maintained in a second

independent facility (Supplementary Figure 4). Altogether, these data suggest that the relative CD5 levels set by the thymic selection threshold are maintained on $CD4^+$ T cells and Tregs in peripheral and pancreatic lymph nodes, independent of the genetic background, while the expression level of CD5 on naïve $CD8^+$ T cells in NOD mice is slightly increased in the periphery relative to B6 mice.

Non-MHC factors are responsible for differences in CD5 expression on $CD44^{hi}$ $CD8^+$ T cells in NOD mice

Naive $CD5^{hi}$ T cells preferentially expand after activation and predominate in the memory compartment [27, 42]. Consistent with this, both $CD44^{hi}$ $CD4^+$ and $CD44^{hi}$ $CD8^+$ T cells express higher levels of CD5 than the respective naïve T cell subset in the three mouse strains tested (Supplementary Figure 3b). Interestingly, as observed in the naïve $CD4^+$ T cell compartment, $CD44^{hi}CD4^+$ T cells from $B6^{g7}$ and NOD mice also express lower levels of CD5 than those from B6 mice, suggesting that differences in CD5 levels are maintained in the MHC class II-restricted T cell compartments and are likely driven by the MHC locus (Figure 2d, e). In contrast to $CD4^+$ T cells, $CD44^{hi}CD8^+$ T cells from the peripheral lymph nodes of NOD mice showed significantly higher levels of CD5 than those from both B6 and $B6^{g7}$ mice (Figure 2d, e). The higher levels of CD5 on $CD44^{hi}$ NOD $CD8^+$ T cells is primarily due to a shift in the global level of CD5 expression as the CV of CD5 is not increased on the $CD44^{hi}CD8^+$ T cells from the peripheral lymph nodes (Figure 2f). The accumulation of $CD44^{hi}CD8^+$ T cells expressing higher levels of CD5 in NOD mice does not appear to be driven by the MHC locus, since the level of expression of CD5 on $CD44^{hi}CD8^+$ T cells is comparable for both B6 and $B6^{g7}$ mice (Figure 2d, e). Altogether, these results suggest that both naïve and $CD44^{hi}CD4^+$ T cells from $B6^{g7}$ and NOD mice include more T cells expressing lower levels of CD5 than B6 mice, which may be reflective of a $CD4^+$ T cell pool with lower basal reactivity to self-antigen. Moreover, although CD5 levels on $CD8^+$ SP thymocytes are comparable among the different mouse strains, a greater number of naïve and $CD44^{hi}CD8^+$ T cells with higher levels of cell surface CD5 are found in the peripheral lymph nodes of NOD mice.

The variation in CD5 expression on T cells is not driven by a subclinical inflammatory response in NOD mice

NOD mice exhibit some degree of insulitis prior to the clinical signs of diabetes [8, 20]. Therefore, we sought to determine whether the differences in CD5 levels observed on thymocytes and T cells

in B6, B6^{g7}, and NOD mice are a consequence of the potential subclinical inflammatory response in NOD mice and whether the findings can be extended to other mouse strains. As such, we quantified CD5 expression on thymocytes and lymph node T cells from B6, NOD, NOR, 129S, A/J, BALB/c, FVB, and C3H mice. Notably, NOR mice are 88% identical by descent to NOD mice and have the same MHC locus as NOD, but they are diabetes resistant [46]. Comparison of these eight strains reveal that NOD and NOR mice show the lowest level of CD5 expression on CD4$^+$ SP thymocytes, tTregs, peripheral CD4$^+$ T cells and Tregs, whereas FVB have the highest (Figure 3a-c and Supplementary Figure 5). As both NOD and NOR strains bear the same MHC locus, these results further suggest variations in CD5 expression levels we observe in CD4$^+$ SP thymocytes and peripheral CD4$^+$ T cells and Tregs is largely driven by the MHC locus. These data also show that FVB, and to a certain extent, C3H background tend to promote the differentiation of thymocytes expressing higher levels of CD5, and that these higher levels are maintained in periphery (Figure 3a-c and Supplementary Figure 5). It remains to be seen if these differences are driven by the MHC locus or other genetic differences.

Although NOR mice are diabetes-resistant, they still show inflammatory immunological phenotypes [46-48]. To unequivocally address the impact of the potential subclinical inflammatory response in NOD mice, we next generated competitive bone marrow chimeras. We reconstituted irradiated F1^{g7} (B6^{g7} x NOD) recipients with a 1:1 mixture of B6^{g7} and NOD bone marrow cells. In this setting, both B6^{g7} and NOD hematopoietic precursors develop in the same environment, also allowing identification of cell-intrinsic traits. As for the parental B6^{g7} and NOD strains (Figures 1 and 2), thymocyte subsets (CD8$^+$ SP, CD4$^+$ SP, and tTregs) and naïve CD4$^+$ T cells of either B6^{g7} or NOD origin in the F1^{g7} chimera expressed similar levels of CD5 (Supplementary Figure 6). In addition, CD5 levels were slightly higher in CD44^{hi}CD4$^+$ T cells and Tregs from NOD mice relative to B6^{g7} mice (Supplementary Figure 6). Moreover, both NOD-derived naïve and CD44^{hi} CD8$^+$ T cells had higher levels of CD5 than those of B6^{g7} origin in the competitive bone marrow chimera setting (Figure 3d-f). This demonstrates that NOD CD8$^+$ T cells that perceive stronger basal TCR signals are favoured in the periphery. Altogether, these data show that the relative CD5 levels on T cells is MHC-independent, T cell-intrinsic, and is not a consequence of differences in inflammatory state, as the cells co-exist in the same host.

CD5 levels on T cells in NOD mice are associated with functional biases

In B6 mice, differences in the strength of basal TCR interactions with self-peptide influence the contribution of naive T cells to an immune response. For example, naïve $CD4^+$ T cells with relatively lower levels of CD5 ($CD5^{lo}$) produce more IFN-γ upon stimulation than those with relatively higher levels of CD5 ($CD5^{hi}$) [49], while naïve $CD5^{hi}$ $CD8^+$ T cells already express higher levels of markers associated with $CD8^+$ T cell activation and differentiation even at steady state (e.g. Eomes) and dominate in the response to antigen challenge [42]. However, this has yet to be tested in NOD mice. Analysis of $CD4^+$ T cells from NOD mice reveals that $CD5^{lo}$ $CD4^+$ T cells produce less IL-2 and more IFN-γ than their $CD5^{hi}$ counterparts (Figure 4a-d and Supplementary Figure 7). We also detect higher expression of Eomes in naïve $CD5^{hi}$ $CD8^+$ T cells relative to $CD5^{lo}$ $CD8^+$ T cells (Figure 4e, f). In NOD mice, the increased proportion of $CD5^{lo}$ $CD4^+$ T cells producing more IFN-γ and the accumulation of $CD5^{hi}$ $CD8^+$ T cells expressing high levels of Eomes may contribute to the increased susceptibility to autoimmune diabetes.

Discussion

In this study, we quantified cell surface expression of CD5 as a reflection of TCR signal strength in thymocytes and peripheral T cells of B6 and NOD mice. Our results demonstrate that thymocyte differentiation in NOD mice does not facilitate the differentiation of $CD4^+$ SP or $CD8^+$ SP thymocytes that perceive strong TCR signals during development. Instead, NOD mice allow the differentiation of a population of $CD4^+$ SP thymocytes and tTreg with relatively lower CD5 levels, and this difference in CD5 expression is maintained on peripheral T cells in NOD mice relative to B6. In contrast to $CD4^+$ T cells, $CD8^+$ SP thymocytes from B6 and NOD mice expressed comparable levels of CD5 whereas peripheral $CD8^+$ T cells expressed higher levels of CD5 in NOD mice, suggesting preferential survival of $CD8^+$ T cells with a higher TCR responsiveness to self-peptide in autoimmune-prone NOD mice.

In addition to B6 and NOD mice, we included $B6^{g7}$ mice in our study in order to discriminate between MHC-dependent and -independent traits. Indeed, among the genetic loci associated with diabetes susceptibility, the MHC locus represents the strongest risk factor for autoimmune diabetes [8, 20, 50, 51]. We observed that the levels of CD5 on $CD4^+$ SP thymocytes and naïve $CD4^+$ T cells is comparable between $B6^{g7}$ and NOD, as well as in NOR mice; these strains allow the differentiation and survival of $CD4^+$ T cells with lower expression of CD5 relative to the B6 strain. This likely reflects the instability of the peptide-I-A^{g7} MHC complex [31-33], and represents a striking difference in the thymic selection of $CD4^+$ SP thymocytes perceiving low TCR signals between the B6 and NOD backgrounds.

Low-affinity T cells have been implicated in the development of several autoimmune diseases [52, 53]. For instance, in a model of multiple sclerosis, while less than 15% of $CD4^+$ T cells specific to myelin oligodendrocyte glycoprotein (MOG) infiltrating the central nervous system are detected by a MOG-MHC-II tetramer staining, a more sensitive 2D TCR affinity analysis revealed that the majority of the infiltrating $CD4^+$ T cells are MOG-specific; they simply exhibit 10- to 100- fold lower affinity to MOG peptide than the MOG-MHC-II $tetramer^+$ T cells [54]. These low affinity $CD4^+$ T cells produce a substantial amount of IFN-γ during experimental autoimmune encephalomyelitis [54]. Interestingly, we have recently shown that murine naïve $CD4^+$ T cells

expressing lower levels of CD5 produce more IFN-γ upon stimulation [49]. In addition, $CD5^{lo}$ tTreg have a lower capacity for maintaining lymphocyte homeostasis in the peripheral LNs relative to their $CD5^{hi}$ tTreg counterparts [55]. Thus, it is conceivable that the development of $CD4^+$ T cells and tTreg with lower CD5 levels are prone to contribute to autoimmune diabetes in NOD mice by producing more IFN-γ and inefficiently regulating autoreactive T cell activity, respectively.

In contrast to peripheral $CD4^+$ T cells, $CD8^+$ T cells express higher levels of CD5 in NOD mice relative to both B6 and $B6^{g7}$ mice and $CD5^{hi}CD8^+$ cells express higher levels of Eomes, suggesting that they may be more cytotoxic. A recent study shows that low levels of MHC-I expression can result in the preferential accumulation of $CD8^+$ T cells expressing higher levels of CD5 [56]. As $B6^{g7}$ and NOD mice carry the same MHC locus, potential differences in MHC-I expression may be driven by polymorphisms in *B2m* [57]. However, we find that the difference in CD5 levels persists in competitive bone marrow chimeras where cells of $B6^{g7}$ and NOD origin co-exist in the same environment and are thus exposed to the same level of MHC. Therefore, the accumulation of $CD8^+$ T cells expressing higher levels of CD5 in NOD mice is not the result of a bias in thymocyte selection, is cell-intrinsic and is MHC-independent. The reason why these $CD5^{hi}$ $CD8^+$ T cells accumulate in the lymph nodes is unclear. Naïve $CD8^+$ T cells with higher CD5 levels may be poised for faster activation that can lead to their preferential expansion [42, 58, 59]. Alternatively, $CD8^+$ T cells with higher affinity to self-peptide MHC may have an intrinsic advantage to survive in the periphery in NOD mice as compared to B6 mice [60-62]. Of relevance, high levels of CD5 on $CD8^+$ T cells is not sufficient to cause spontaneous autoimmune phenotypes, as $CD8^+$ T cells in both FVB and C3H strains express even higher levels of CD5 than in the NOD strain.

In conclusion, our study reveals, based on cell surface CD5 levels, that polyclonal conventional T cells and Tregs generated in NOD mice do not perceive stronger TCR signals during development than those in diabetes resistant B6 mice. Instead, we find that the $H\text{-}2^{g7}$ locus facilitates the differentiation of $CD4^+$ T cells and tTreg expressing low levels of CD5 that may contribute to the autoimmune process. Moreover, we observed preferential survival of peripheral NOD $CD8^+$ T cells with higher CD5 levels, suggesting a higher reactivity to self-peptide MHC. Thus, this work confirms and expands upon previous studies using monoclonal TCR transgenic mouse strains to

296 suggest that thymic selection and peripheral T cell homeostasis is altered in NOD mice with
297 important implications in the development of autoimmunity.
298

Methods

Mice

All mice were maintained in specific pathogen free animal facilities either at the Maisonneuve-Rosemont Hospital Research Center or at the University of Alberta Health Sciences and Laboratory Animal Services. NOD/SHiLtJ (NOD, #001976), C57BL/6 (B6, #000664), B6.SJL-Ptprc^{a}Pepc^{b}/BoyJ (B6.SJL, #002014), B6.NOD-(D17Mit21-D17Mit10)/LtJ (B6^{g7}, #003300), NOR/LtJ (#002050), 129S1/SvImJ (#002448), A/J (#000646), BALB/cJ (#000651), FVB/NJ (#001800), and C3H/HeJ (#000659) were purchased from the Jackson Laboratory (Bar Harbor, ME, USA). B6 x B6SJL (CD45.1.2 B6) and NOD x B6^{g7} F1 (F1^{g7}) were bred in house. B6.Rag2pGFP (B6.Rag-GFP) mice [63, 64] were kindly provided by Pamela Fink (University of Washington, Seattle, WA, USA) and bred in house and were crossed to NOD mice for more than 14 generations to generate NOD.Rag-GFP mice. Both male and female mice aged 6 - 9 weeks were used except as noted. All protocols have been approved by the Animal Care Committee at Maisonneuve-Rosemont Hospital Research Centre and the Animal Care and Use Committee Health Sciences of the University of Alberta. Experiments were performed in accordance with the Canadian Council on Animal Care guidelines.

Antibodies and Flow Cytometry

Fluorescently labelled anti-mouse CD4 (RM4-5 and GK1.5), CD8α (53-6.7), CD25 (PC61), CD44 (IM7), CD45.1 (A20), CD45.2 (104), CD62L (MEL-14), TCRβ (H57-597), CD73 (RTY/11.8), CD5 (53-7.3), interleukin-2 (IL-2; JES6-5H4), interferon-gamma (IFN-γ; XMG1.2), and Zombie fixable viability dye were purchased from BioLegend (San Diego, CA, USA); anti-mouse CD5 (53-7.3) was purchased from BD Biosciences (San Jose, CA, USA); and anti-FoxP3 (150D/E4) and Eomes (Dan11mag) were purchased from eBioscience (Thermo Fisher, Waltham, MA, USA). For experiments in Supplementary Figure 4, fluorescently labelled anti-mouse TCRβ (H57-597), CD4 (RM4-5), CD5 (53-7.3) were purchased from eBioscience (Thermo Fisher, Waltham, MA, USA); anti-mouse CD8α (53-6.7) was purchased from BD Biosciences (San Jose, CA, USA). Single-cell suspensions of thymus, peripheral lymph nodes (inguinal, axillary, and brachial), and pancreatic lymph nodes were prepared with glass tissue homogenizers. Red blood cells were lysed with ACK lysis buffer (0.15 M NH_4Cl, 10 mM $KHCO_3$, 0.1 mM Na_2EDTA). Cells were filtered

and counted with hemacytometer using trypan blue. An equivalent number of cells from each organ were stained. To block FcR, peripheral lymphocytes were first incubated with 2.4G2 supernatant or a cocktail (containing normal mouse, rat, and hamster serum, and 2.4G2) for 10 min at 4°C. Cells were then incubated with viability dye (or debris/dead cells excluded by FSC/SSC gating for Supplementary Figure 4) according to the manufacturer's protocol followed by incubation with cell surface antibodies for 20 minutes at 4°C. To stain for FoxP3 and Eomes, cells were fixed and permeabilized using a FoxP3 Staining Kit (eBioscience/Thermo Fisher, Waltham, MA, USA) according to the manufacturer's protocol. To stain for cytokines, cells were fixed and permeabilized using Cytofix/Cytoperm Plus Kit (BD Biosciences, San Jose, CA, USA) according to manufacturer's protocol. All data were acquired on an LSRFortessa X-20 or BD LSR II flow cytometer using FACSDiva software and analyzed with FlowJo version 10 (BD Biosciences, San Jose, CA, USA).

Bone marrow chimera

T cells were depleted from 6-8-week-old $B6^{g7}$ (CD45.2) and NOD (CD45.1) donor mice by intraperitoneal injection of 100 µg InVivoMAb anti-mouse Thy1 (BioXcell, Lebanon, NH, USA) at 1 and 2 days prior to harvesting the bone marrow. Donor cells were mixed in a 1:1 ratio after red blood cell lysis, and $2x10^6$ total cells were intravenously injected into sex-matched irradiated (10 Gy) $F1^{g7}$ recipients (6-8 weeks old). To ensure T cells were depleted, the recipient mice received intraperitoneal injection of 100 µg InVivoMAb anti-mouse Thy1 (BioXcell, Lebanon, NH, USA) at 1 and 7 days after bone marrow reconstitution. After 45 days, the thymus, peripheral lymph nodes (inguinal, axillary, and brachial) and pancreatic lymph nodes were harvested and prepared for flow cytometry as described above.

In vitro activation

Cells were suspended in RPMI media (Wisent, St-Bruno, QC, Canada) supplemented with 10% fetal bovine serum (GE Life Sciences, Pittsburgh, PA, USA), 100 IU penicillin, 100 µg mL^{-1} streptomycin and 2 mM L-glutamine (Wisent, St-Bruno, QC, Canada), 10 µM β-mercaptoethanol. For bulk T cell activation, single cell suspensions were incubated for 4 hours in RPMI media containing or not 100 ng mL^{-1} phorbol myristate acetate (PMA, Millipore Sigma, Darmstadt, Germany) and 1 µg mL^{-1} ionomycin (Calbiochem, San Diego, CA, USA) in the presence of 1 µL

361 mL^{-1} Golgi Plug (BD Biosciences, San Jose, CA, USA) prior to analysing cytokine production.
362 For anti-CD3/CD28 activation, naïve $CD4^+$ were enriched (CD4 isolation kit, STEMCELL
363 Technologies, Vancouver, BC, Canada) according to the manufacturer's protocol, and 2-3 x 10^5
364 enriched naïve $CD4^+$ T cells were seeded per well of a 96-well plate. Cells were stimulated with 5
365 $\mu g\ mL^{-1}$ plate-bound anti-CD3 (145- 2C11; BioLegend, San Diego, CA, USA) and 2 $\mu g\ mL^{-1}$
366 soluble anti-CD28 (37.51; BioLegend, San Diego, CA, USA) under Th1 polarizing conditions
367 with 20 ng mL^{-1} recombinant mouse IL-12 (p70) and 1 $\mu g\ mL^{-1}$ anti-mouse IL-4 (11B11;
368 BioLegend, San Diego, CA, USA). Three days later, half of the media was aspirated from each
369 well and replenished with fresh media with 40 ng mL^{-1} recombinant mouse IL-2 for the Th0
370 condition, and both 40 ng mL^{-1} recombinant mouse IL-2 and 2 $\mu g\ mL^{-1}$ anti-mouse IL-4 (11B11,
371 BioLegend, San Diego, CA, USA) for Th1 skewing. On day 5, half of the media was aspirated
372 from each well and replenished with fresh media containing 100 ng mL^{-1} PMA (Millipore Sigma,
373 Darmstadt, Germany) and 2 $\mu g\ mL^{-1}$ ionomycin (Calbiochem, San Diego, CA, USA). Cells were
374 incubated for an additional 4 hours prior to analysing cytokine production.
375
376 *Statistical Analysis*
377 Statistical analyses were performed using Prism version 8 (GraphPad, San Diego, CA, USA). A
378 one-way ANOVA followed by Sidak's multiple comparison test was applied to compare data from
379 B6, $B6^{g7}$ and NOD mice. A one-way ANOVA followed by Dunnett's multiple comparison test
380 was applied to compare data from B6, NOD, NOR, 129S, A/J, BALB/c, FVB, and C3H mice. A
381 paired *t*-test was applied to compare $B6^{g7}$- and NOD-derived cells from individual bone marrow
382 chimeric mouse. Statistical significance is indicated by *P*-values: * $P < 0.05$, ** $P < 0.01$, *** $P <$
383 0.001.
384
385

Acknowledgments

We thank Drs Aditi Sood, Marilaine Fournier, and Marion Dubuissez for critical reading of the manuscript, as well as Dr Nathalie Labrecque and Felix Lombard-Vadnais for thoughtful discussion of the data. We are grateful to Martine Dupuis from the flow cytometry facility as well as all animal house staff for maintaining the mouse colonies as well as Jiaxin Lin for generating NOD.Rag-GFP mice. This work was supported by Canadian Institutes of Health Research (CIHR) grants (PS148588) to CCA and (PJT 398718) to SL, as well as a Liana's Dream Foundation grant to SL and a Diabète Québec grant to HJM. MD is supported by a doctoral training scholarship from the Fonds de la recherche en santé du Québec (FRQ-S). MD and CA received Lucie Besner scholarships for type 1 diabetes. CA is also supported by the Montreal Diabetes Research Center and the Département de microbiologie, infectiologie et immunologie at the University of Montréal. AA was supported by an Alberta Diabetes Institute Blanch graduate award. MEL is supported by FRQ-S and *L'Oréal*-UNESCO For Women in Science post-doctoral fellowships. HJM is a junior 1 scholar of the FRQ-S and a CIHR New Investigator (MSH-141967). SL is an FRQ-S Research Scholars Emeritus awardee.

Conflict of Interest

None.

References

1. Klein L, Kyewski B, Allen PM *et al.* Positive and negative selection of the T cell repertoire: what thymocytes see (and don't see). *Nat Rev Immunol* 2014;**14**:377-391.
2. Klein L, Robey EA, Hsieh CS. Central CD4$^+$ T cell tolerance: deletion versus regulatory T cell differentiation. *Nat Rev Immunol* 2019;**19**:7-18.
3. Hogquist KA, Jameson SC. The self-obsession of T cells: how TCR signaling thresholds affect fate 'decisions' and effector function. *Nat Immunol* 2014;**15**:815-823.
4. Ramsdell F, Lantz T, Fowlkes BJ. A nondeletional mechanism of thymic self tolerance. *Science* 1989;**246**:1038-1041.
5. Hu QN, Suen AYW, Henao Caviedes LM *et al.* Nur77 Regulates nondeletional mechanisms of tolerance in T cells. *J Immunol* 2017;**199**:3147-3157.
6. Labrecque N, Baldwin T, Lesage S. Molecular and genetic parameters defining T-cell clonal selection. *Immunol Cell Biol* 2011;**89**:16-26.
7. Cheng M, Anderson MS. Thymic tolerance as a key brake on autoimmunity. *Nat Immunol* 2018;**19**:659-664.
8. Mullen Y. Development of the nonobese diabetic mouse and contribution of animal models for understanding type 1 diabetes. *Pancreas* 2017;**46**:455-466.
9. Chen YG, Mathews CE, Driver JP. The role of NOD mice in type 1 diabetes research: lessons from the past and recommendations for the future. *Front Endocrinol (Lausanne)* 2018;**9**:51.
10. Kishimoto H, Sprent J. A defect in central tolerance in NOD mice. *Nat Immunol* 2001;**2**:1025-1031.
11. Villunger AM, V.S.; Strasser, A. Efficient T cell receptor–mediated apoptosis in nonobese diabetic mouse thymocytes. *Nat Immunol* 2003;**4**:718.
12. Lesage S, Hartley SB, Akkaraju S *et al.* Failure to censor forbidden clones of CD4 T cells in autoimmune diabetes. *J Exp Med* 2002;**196**:1175-1188.
13. Serre L, Fazilleau N, Guerder S. Central tolerance spares the private high-avidity CD4$^+$ T-cell repertoire specific for an islet antigen in NOD mice. *Eur J Immunol* 2015;**45**:1946-1956.
14. Zucchelli S, Holler P, Yamagata T *et al.* Defective central tolerance induction in NOD mice: genomics and genetics. *Immunity* 2005;**22**:385-396.
15. Mingueneau M, Jiang W, Feuerer M *et al.* Thymic negative selection is functional in NOD mice. *J Exp Med* 2012;**209**:623-637.

16. Liston A, Lesage S, Gray DH *et al.* Generalized resistance to thymic deletion in the NOD mouse; a polygenic trait characterized by defective induction of Bim. *Immunity* 2004;**21**:817-830.
17. Kanagawa OS, J.; Vaupel, B.A. Thymic and postthymic regulation of diabetogenic CD8 T cell development in TCR transgenic nonobese diabetic (NOD) mice. *J Immunol* 2000;**164**:5466-5473.
18. DiLorenzo TP, Graser RT, Ono T *et al.* Major histocompatibility complex class I-restricted T cells are required for all but the end stages of diabetes development in nonobese diabetic mice and use a prevalent T cell receptor α chain gene rearrangement. *Proc Natl Acad Sci U S A* 1998;**95**:12538-12543.
19. Choisy-Rossi CM, Holl TM, Pierce MA *et al.* Enhanced pathogenicity of diabetogenic T cells escaping a non-MHC gene-controlled near death experience. *J Immunol* 2004;**173**:3791-3800.
20. Anderson MS, Bluestone JA. The NOD mouse: a model of immune dysregulation. *Annu Rev Immunol* 2005;**23**:447-485.
21. Maier LM, Wicker LS. Genetic susceptibility to type 1 diabetes. *Curr Opin Immunol* 2005;**17**:601-608.
22. Ridgway WM, Peterson LB, Todd JA *et al.* Gene-gene interactions in the NOD mouse model of type 1 diabetes. *Adv Immunol* 2008;**100**:151-175.
23. Delovitch TL, Singh B. The nonobese diabetic mouse as a model of autoimmune diabetes: immune dysregulation gets the NOD. *Immunity* 1997;**7**:727-738.
24. Unanue ER, Wan X. The immunoreactive platform of the pancreatic islets influences the development of autoreactivity. *Diabetes* 2019;**68**:1544-1551.
25. Calderon B, Carrero JA, Unanue ER. The central role of antigen presentation in islets of Langerhans in autoimmune diabetes. *Curr Opin Immunol* 2014;**26**:32-40.
26. Azzam HS, Grinberg A, Lui K *et al.* CD5 expression is developmentally regulated by T cell receptor (TCR) signals and TCR avidity. *J Exp Med* 1998;**188**:2301-2311.
27. Mandl JN, Monteiro JP, Vrisekoop N *et al.* T cell-positive selection uses self-ligand binding strength to optimize repertoire recognition of foreign antigens. *Immunity* 2013;**38**:263-274.
28. Smith K, Seddon B, Purbhoo MA *et al.* Sensory adaptation in naive peripheral CD4 T cells. *J Exp Med* 2001;**194**:1253-1261.

29. Persaud SP, Parker CR, Lo WL *et al.* Intrinsic $CD4^+$ T cell sensitivity and response to a pathogen are set and sustained by avidity for thymic and peripheral complexes of self peptide and MHC. *Nat Immunol* 2014;**15**:266-274.

30. Cho JH, Kim HO, Ju YJ *et al.* CD45-mediated control of TCR tuning in naive and memory $CD8^+$ T cells. *Nat Commun* 2016;**7**:13373.

31. Carrasco-Marin E, Shimizu J, Kanagawa O *et al.* The class II MHC I-A^{g7} molecules from non-obese diabetic mice are poor peptide binders. *J Immunol* 1996;**156**:450-458.

32. Kanagawa O, Martin SM, Vaupel BA *et al.* Autoreactivity of T cells from nonobese diabetic mice: an I-A^{g7}-dependent reaction. *Proc Natl Acad Sci U S A* 1998;**95**:1721-1724.

33. Latek RR, Suri A, Petzold SJ *et al.* Structural basis of peptide binding and presentation by the type I diabetes-associated MHC class II molecule of NOD mice. *Immunity* 2000;**12**:699-710.

34. Yui MA, Muralidharan K, Moreno-Altamirano B *et al.* Production of congenic mouse strains carrying NOD-derived diabetogenic genetic intervals: an approach for the genetic dissection of complex traits. *Mamm Genome* 1996;**7**:331-334.

35. Collin R, Balmer L, Morahan G *et al.* Common heritable immunological variations revealed in genetically diverse inbred mouse strains of the Collaborative Cross. *J Immunol* 2019;**202**:777-786.

36. Berzins SP, Venanzi ES, Benoist C *et al.* T-cell compartments of prediabetic NOD mice. *Diabetes* 2003;**52**:327-334.

37. Collin R, Lombard-Vadnais F, Hillhouse EE *et al.* MHC-independent thymic selection of CD4 and CD8 coreceptor negative αβ T Cells. *J Immunol* 2020;**205**:133-142.

38. Ordonez-Rueda D, Lozano F, Sarukhan A *et al.* Increased numbers of thymic and peripheral $CD4^+$ $CD25^+Foxp3^+$ cells in the absence of CD5 signaling. *Eur J Immunol* 2009;**39**:2233-2247.

39. Owen DL, Mahmud SA, Sjaastad LE *et al.* Thymic regulatory T cells arise via two distinct developmental programs. *Nat Immunol* 2019;**20**:195-205.

40. Thiault N, Darrigues J, Adoue V *et al.* Peripheral regulatory T lymphocytes recirculating to the thymus suppress the development of their precursors. *Nat Immunol* 2015;**16**:628-634.

41. Darrigues J, Santamaria JC, Galindo-Albarran A *et al.* Robust intrathymic development of regulatory T cells in young NOD mice is rapidly restrained by recirculating cells. *Eur J Immunol* 2020e-pub ahead of print Jul 30;10.1002/eji.202048743.

42. Fulton RB, Hamilton SE, Xing Y *et al.* The TCR's sensitivity to self peptide-MHC dictates the ability of naive $CD8^+$ T cells to respond to foreign antigens. *Nat Immunol* 2015;**16**:107-117.
43. Fry TJ, Mackall CL. The many faces of IL-7: from lymphopoiesis to peripheral T cell maintenance. *J Immunol* 2005;**174**:6571-6576.
44. Surh CD, Sprent J. Homeostasis of naive and memory T cells. *Immunity* 2008;**29**:848-862.
45. Takada K, Jameson SC. Naive T cell homeostasis: from awareness of space to a sense of place. *Nat Rev Immunol* 2009;**9**:823-832.
46. Prochazka M, Serreze DV, Frankel WN *et al.* NOR/Lt mice: MHC-matched diabetes-resistant control strain for NOD mice. *Diabetes* 1992;**41**:98-106.
47. Fox CJ, Danska JS. Independent genetic regulation of T-cell and antigen-presenting cell participation in autoimmune islet inflammation. *Diabetes* 1998;**47**:331-338.
48. Ivakine EA, Fox CJ, Paterson AD *et al.* Sex-specific effect of insulin-dependent diabetes 4 on regulation of diabetes pathogenesis in the nonobese diabetic mouse. *J Immunol* 2005;**174**:7129-7140.
49. Sood A, Lebel ME, Fournier M *et al.* Differential interferon-gamma production potential among naive $CD4^+$ T cells exists prior to antigen encounter. *Immunol Cell Biol* 2019;**97**:931-940.
50. Prochazka M, Leiter EH, Serreze DV *et al.* Three recessive loci required for insulin-dependent diabetes in nonobese diabetic mice. *Science* 1987;**237**:286-289.
51. Polychronakos C, Li Q. Understanding type 1 diabetes through genetics: advances and prospects. *Nat Rev Genet* 2011;**12**:781-792.
52. Zehn D, Bevan MJ. T cells with low avidity for a tissue-restricted antigen routinely evade central and peripheral tolerance and cause autoimmunity. *Immunity* 2006;**25**:261-270.
53. Liu GY, Fairchild PJ, Smith RM *et al.* Low avidity recognition of self-antigen by T cells permits escape from central tolerance. *Immunity* 1995;**3**:407-415.
54. Sabatino JJ, Jr., Huang J, Zhu C *et al.* High prevalence of low affinity peptide-MHC II tetramer-negative effectors during polyclonal $CD4^+$ T cell responses. *J Exp Med* 2011;**208**:81-90.
55. Wyss L, Stadinski BD, King CG *et al.* Affinity for self antigen selects Treg cells with distinct functional properties. *Nat Immunol* 2016;**17**:1093-1101.
56. Sng XYX, Li J, Zareie P *et al.* The Impact of MHC Class I Dose on Development and Maintenance of the Polyclonal Naive $CD8^+$ T Cell Repertoire. *J Immunol* 2020;**204**:3108-3116.

57. Hamilton-Williams EE, Serreze DV, Charlton B *et al.* Transgenic rescue implicates β2-microglobulin as a diabetes susceptibility gene in nonobese diabetic (NOD) mice. *Proc Natl Acad Sci U S A* 2001;**98**:11533-11538.

58. Cho JH, Kim HO, Surh CD *et al.* T cell receptor-dependent regulation of lipid rafts controls naive $CD8^+$ T cell homeostasis. *Immunity* 2010;**32**:214-226.

59. Palmer MJ, Mahajan VS, Chen J *et al.* Signaling thresholds govern heterogeneity in IL-7-receptor-mediated responses of naive $CD8^+$ T cells. *Immunol Cell Biol* 2011;**89**:581-594.

60. Lamhamedi-Cherradi SE, Luan JJ, Eloy L *et al.* Resistance of T-cells to apoptosis in autoimmune diabetic (NOD) mice is increased early in life and is associated with dysregulated expression of Bcl-x. *Diabetologia* 1998;**41**:178-184.

61. Ryan KR, McCue D, Anderton SM. Fas-mediated death and sensory adaptation limit the pathogenic potential of autoreactive T cells after strong antigenic stimulation. *J Leukoc Biol* 2005;**78**:43-50.

62. Axtell RC, Webb MS, Barnum SR *et al.* Cutting edge: critical role for CD5 in experimental autoimmune encephalomyelitis: inhibition of engagement reverses disease in mice. *J Immunol* 2004;**173**:2928-2932.

63. Yu W, Nagaoka H, Jankovic M *et al.* Continued RAG expression in late stages of B cell development and no apparent re-induction after immunization. *Nature* 1999;**400**:682-687.

64. Boursalian TE, Golob J, Soper DM *et al.* Continued maturation of thymic emigrants in the periphery. *Nat Immunol* 2004;**5**:418-425.

Figure Captions

Figure 1. NOD thymocytes do not perceive stronger TCR signals than their B6 counterparts. (**a**) Representative histograms of CD5 expression on the indicated thymocyte subsets from B6 (grey shaded), $B6^{g7}$ (dotted line), and NOD (solid line) mice. The thymocyte subset gating strategy is shown in Supplementary Figure 1a. (**b**) CD5 relative fluorescent intensities (RFI) and (**c**) CD5 coefficient of variation (CV) on $CD8^+$ SP, $CD4^+$ SP and tTregs from B6, $B6^{g7}$, and NOD mice. The RFI is calculated by normalizing to the average of the CD5 mean fluorescent intensity (MFI) on $CD8^+$ SP thymocytes from B6 mice in each experiment. Each dot depicts data from an individual mouse; B6 (n=9), $B6^{g7}$ (n=11), NOD (n=10). The data was obtained in four independent experiments that included at least one mouse per strain. **(d)** Representative histograms of CD5 expression, and compilation of CD5 RFI and CD5 CV on non-recirculated ($CD73^-$) tTregs from B6 (grey shaded), $B6^{g7}$ (dotted line), and NOD (solid line) mice. The CD5 RFI is calculated by normalizing to the average of the CD5 MFI on $CD4^+$ SP thymocytes from B6 mice in each experiment. Each dot depicts data from an individual mouse; B6 (n=6), $B6^{g7}$ (n=6), NOD (n=6). The data was obtained in two independent experiments that included at least one mouse per strain. One-way ANOVA followed by Sidak's multiple comparison test, * $P < 0.05$, ** $P < 0.01$, *** $P < 0.001$.

Figure 2. The differential expression of CD5 is maintained on peripheral $CD4^+$ T cells and increased on $CD8^+$ T cells in NOD relative to B6 mice. The T cell gating strategy is shown in Supplementary Figure 3a. (**a**) Representative histograms of CD5 expression on the indicated T cell subsets from B6 (grey shaded), $B6^{g7}$ (dotted line), and NOD (solid line) mice from peripheral lymph nodes. (**b**) CD5 RFI and (**c**) CD5 CV on naïve $CD8^+$ and $CD4^+$ T cells as well as Treg from peripheral and pancreatic lymph nodes of B6, $B6^{g7}$, and NOD mice. (**d**) Representative histograms of CD5 expression on the indicated $CD44^{hi}$ T cell subsets from B6, $B6^{g7}$ and NOD mice. (**e**) CD5 RFI and (**f**) CD5 CV on $CD44^{hi}$ $CD8^+$ and $CD44^{hi}$ $CD4^+$ T cells from peripheral and pancreatic lymph nodes of B6, $B6^{g7}$, and NOD mice. The RFI was calculated by normalizing to the average of the CD5 MFI on naïve $CD8^+$ T cells from B6 mice in each experiment. Each dot depicts data from an individual mouse from four to six independent experiments that included at least one mouse per strain; peripheral lymph nodes: B6 (n=15), $B6^{g7}$ (n=17), NOD (n=16); pancreatic lymph

nodes: B6 (n=9), B6^{g7} (n=11), NOD (n=7). One-way ANOVA followed by Sidak's multiple comparison test, * $P < 0.05$, ** $P < 0.01$, *** $P < 0.001$.

Figure 3. Increased CD5 expression on NOD CD8$^+$ T cells is not driven by a subclinical inflammatory response. The T cells were gated using strategy shown in Supplementary Figures 1a, 2f, and 3a. CD5 RFI on **(a)** CD8$^+$ SP, CD73$^-$ CD4$^+$ SP thymocytes, as well as CD73$^-$ tTregs, **(b)** naïve CD8$^+$, naïve CD4$^+$ and Tregs from the peripheral lymph nodes, and **(c)** CD44^{hi} CD8$^+$ and CD44^{hi} CD4$^+$ from the peripheral lymph nodes for the indicated mouse strains. The RFI is calculated by normalizing to the CD5 MFI on CD8$^+$ SP thymocytes or naïve CD8$^+$ T cells from a co-stained CD45.1.2 B6 mouse in each sample. Each dot depicts data from an individual mouse; n=5 for each strain. The data was obtained in two independent experiments that included at least one mouse per strain. One-way ANOVA followed by Dunnett's multiple comparison test where each strain is compared to C57BL/6, * $P < 0.05$, ** $P < 0.01$, *** $P < 0.001$. (**d**) Bone marrow cells isolated from B6^{g7} (CD45.2) and NOD (CD45.1) mice were injected at a 1:1 ratio into lethally irradiated F1^{g7} (B6^{g7} x NOD, CD45.1.2) mice. Representative histograms of CD5 expression on B6^{g7}- (dotted line) and NOD- (solid line) derived naïve CD8$^+$ T cells (TCRβ$^+$ CD8$^+$ CD62L$^+$ CD44$^-$) and CD44^{hi} CD8$^+$ T cells (TCRβ$^+$ CD8$^+$ CD44$^+$) from peripheral lymph nodes. (**e**) CD5 RFI and (**f**) CD5 CV on B6^{g7}- or NOD-derived naïve and CD44^{hi} CD8$^+$ T cells from peripheral and pancreatic lymph nodes. The RFI was calculated by normalizing to the average of the CD5 MFI on B6^{g7} derived naïve or CD44^{hi} CD8$^+$ T cells in each experiment. Each dot indicates data from cells of either B6^{g7} or NOD origin in chimeric mice from two independent experiments; n=9 recipients. Paired *t*-test, ** $P < 0.01$, *** $P < 0.001$.

Figure 4. CD5^{lo} and CD5^{hi} naïve CD4$^+$ and CD8$^+$ T cells in NOD mice are poised to different functions. **(a)** Representative flow plots depicting gating strategies for PMA/ionomycin activated TCRβ$^+$ CD4$^+$ T cells with low expression of CD44 (naïve CD4$^+$). Naïve CD4$^+$ T cells were subsequently gated on the top and bottom 20% of CD5 expression to examine IL-2 production. **(b)** Percentage of IL-2$^+$ cells gated on CD5^{lo} and CD5^{hi} naïve CD4$^+$ T cells, based on unstimulated controls. Each dot indicates individual mice from two independent experiments, n=6 mice, and averages of technical triplicates are shown. Lines join samples from CD5^{lo} and CD5^{hi} compartments from the same mice. **(c)** Representative flow plots depicting gating strategies of

IFN-γ production from $CD5^{lo}$ and $CD5^{hi}$ enriched naïve $CD4^+$ T cells activated with anti-CD3/CD28 under Th1 skewing condition. **(d)** Percentage of IFN-γ^+ cells gated on $CD5^{lo}$ and $CD5^{hi}$ activated $CD4^+$ $CD25^+$ T cells. Each dot indicates individual experiments, averages of technical triplicates are shown, and lines join samples from $CD5^{lo}$ and $CD5^{hi}$ compartments from the same experiment. n=3 mice in three individual experiments. **(e)** Representative histograms depicting top and bottom 20% of CD5 expression on naïve $CD8^+$ T cells to compare Eomes expression by $CD5^{lo}$ and $CD5^{hi}$ naïve $CD8^+$ T cells with $CD44^{hi}$ $CD8^+$ T cells. **(f)** RFI of Eomes on $CD5^{lo}$ and $CD5^{hi}$ naïve $CD8^+$ T cells. Each dot depicts data from an individual mouse from two independent experiments; n=6 mice. Paired student *t*-test, * $P < 0.05$, *** $P < 0.001$.

Figure 1

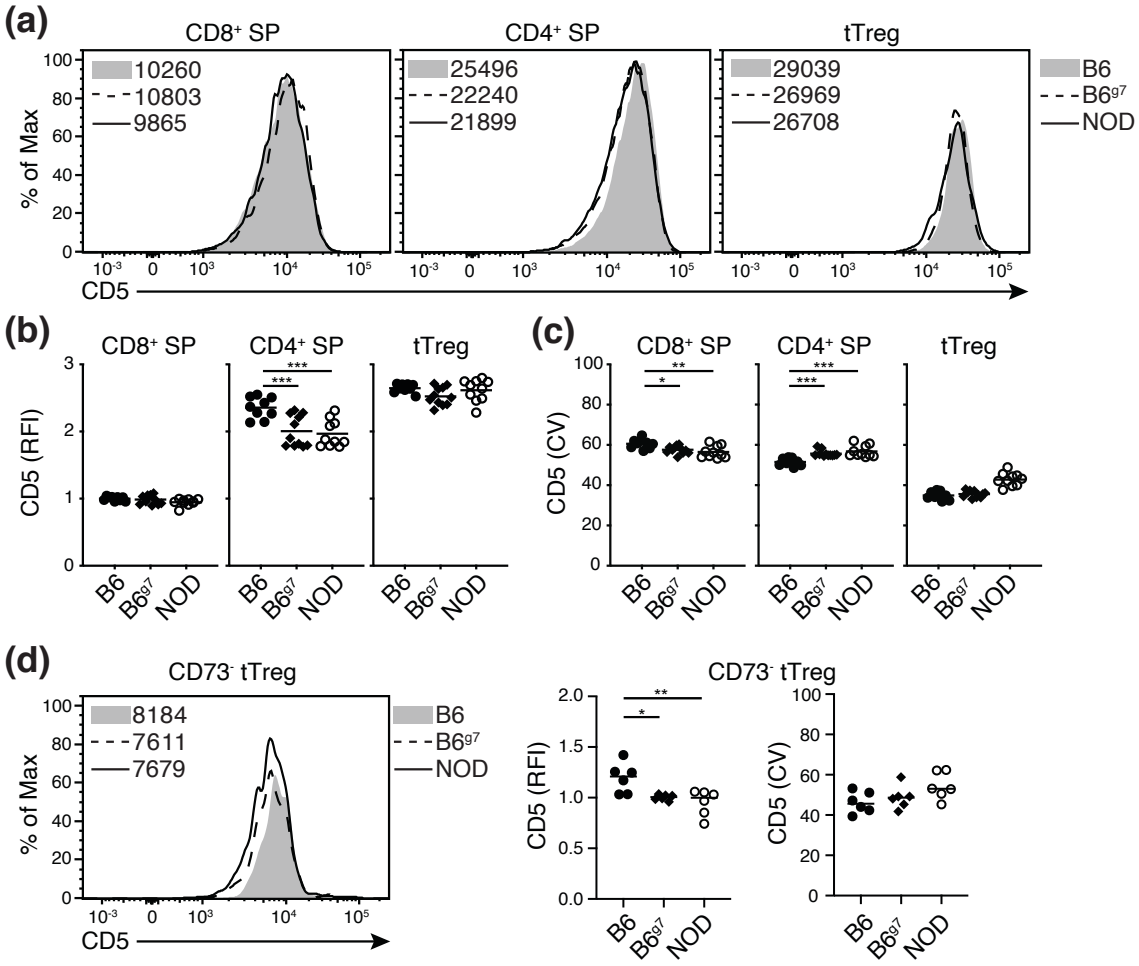
(a)
CD8+ SP
CD4+ SP
tTreg
10260
10803
9865
25496
22240
21899
29039
26969
26708
B6
B6g7
NOD
% of Max
CD5
(b)
CD5 (RFI)
(c)
CD5 (CV)
(d)
CD73- tTreg
8184
7611
7679

Figure 2

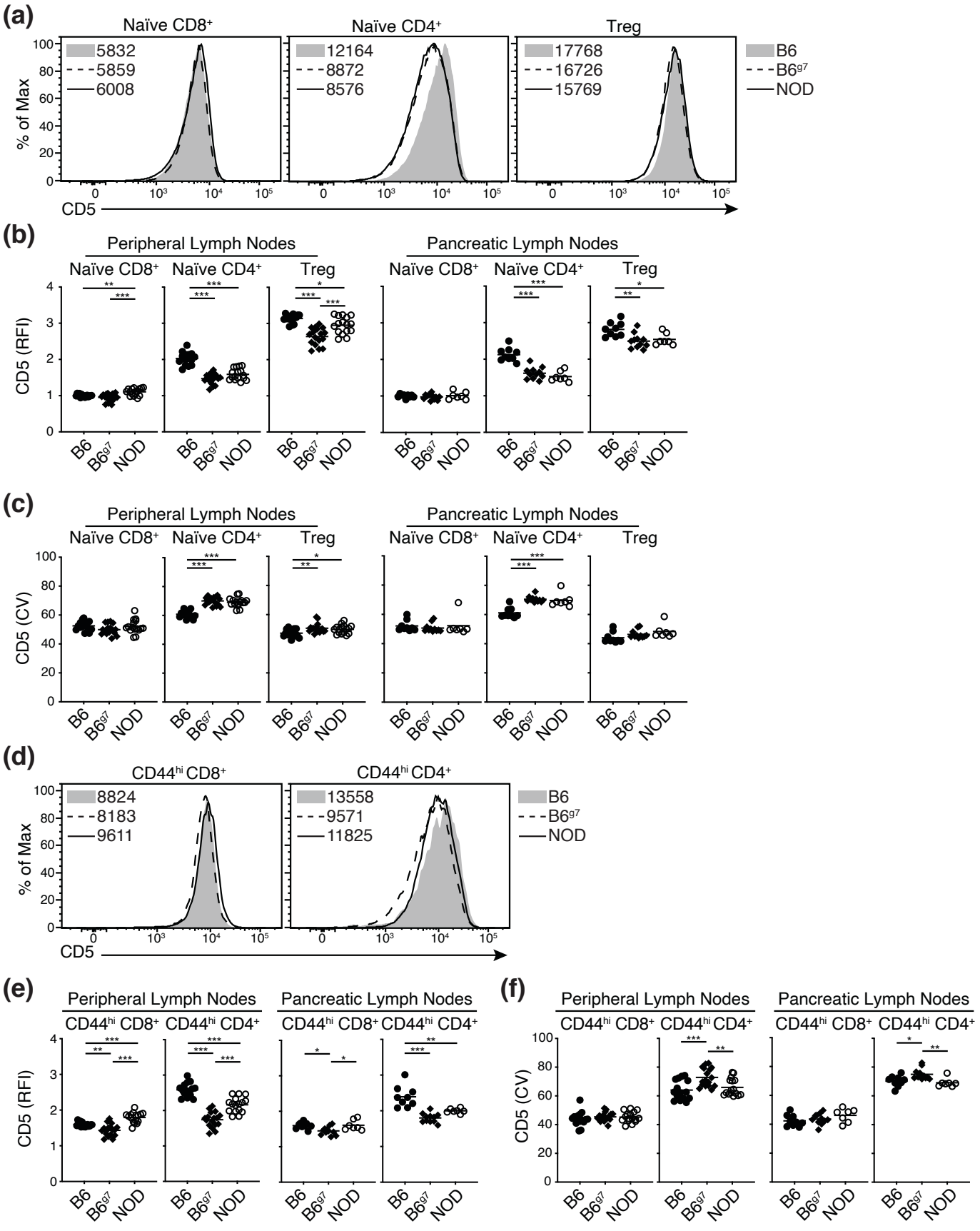
(a)
Naïve CD8+
Naïve CD4+
Treg
5832
5859
6008
12164
8872
8576
17768
16726
15769
B6
B6g7
NOD
% of Max
CD5
(b)
Peripheral Lymph Nodes
Pancreatic Lymph Nodes
Naïve CD8+
Naïve CD4+
Treg
CD5 (RFI)
B6
B6g7
NOD
(c)
CD5 (CV)
(d)
CD44hi CD8+
CD44hi CD4+
8824
8183
9611
13558
9571
11825
(e)
CD44hi CD8+
CD44hi CD4+
(f)

Figure 3

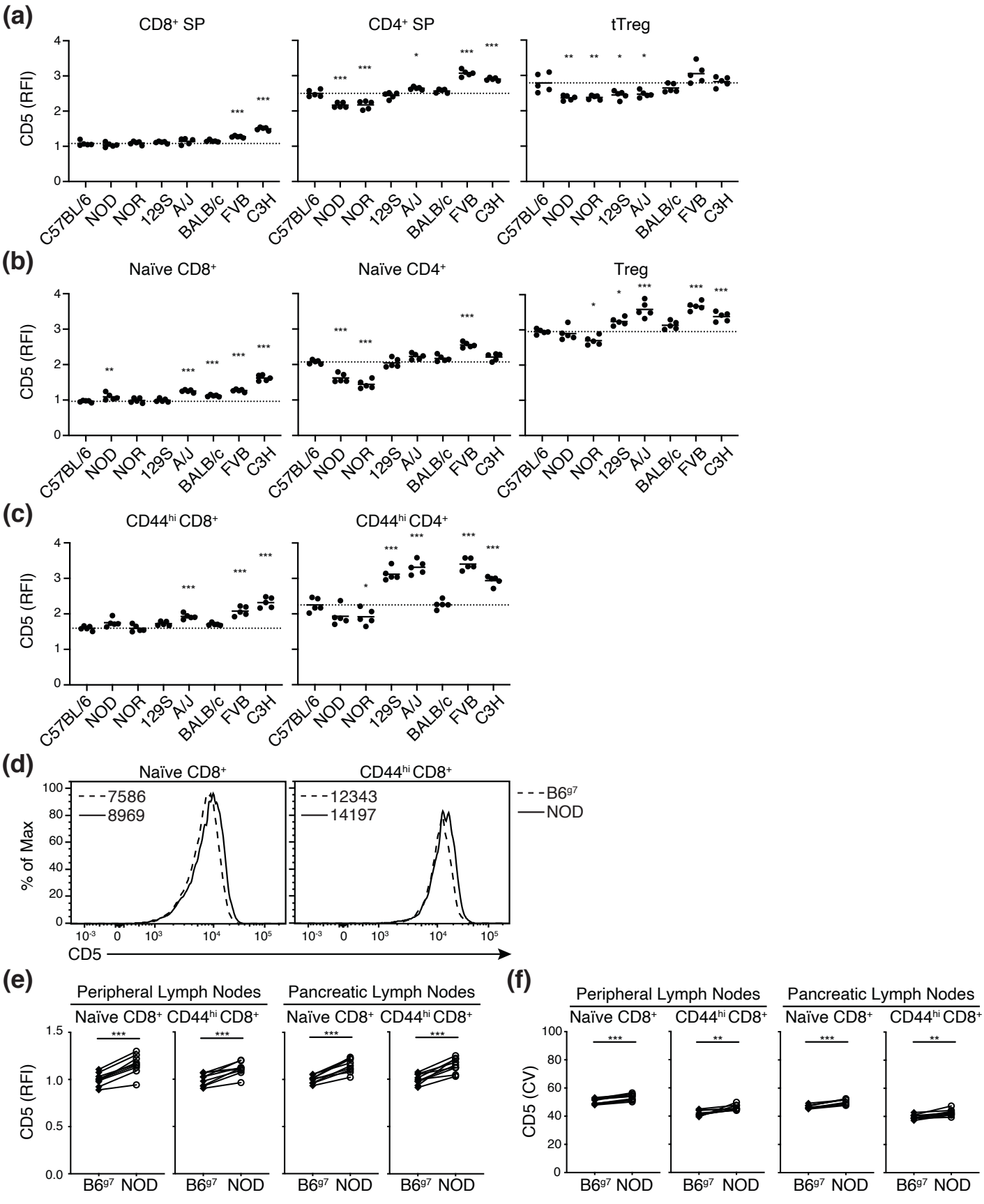
(a)
CD8+ SP
CD4+ SP
tTreg
CD5 (RFI)
C57BL/6
NOD
NOR
129S
A/J
BALB/c
FVB
C3H
(b)
Naïve CD8+
Naïve CD4+
Treg
(c)
CD44hi CD8+
CD44hi CD4+
(d)
Naïve CD8+
CD44hi CD8+
7586
8969
12343
14197
B6g7
NOD
% of Max
CD5
(e)
Peripheral Lymph Nodes
Pancreatic Lymph Nodes
Naïve CD8+
CD44hi CD8+
CD5 (RFI)
B6g7
NOD
(f)
CD5 (CV)

Figure 4

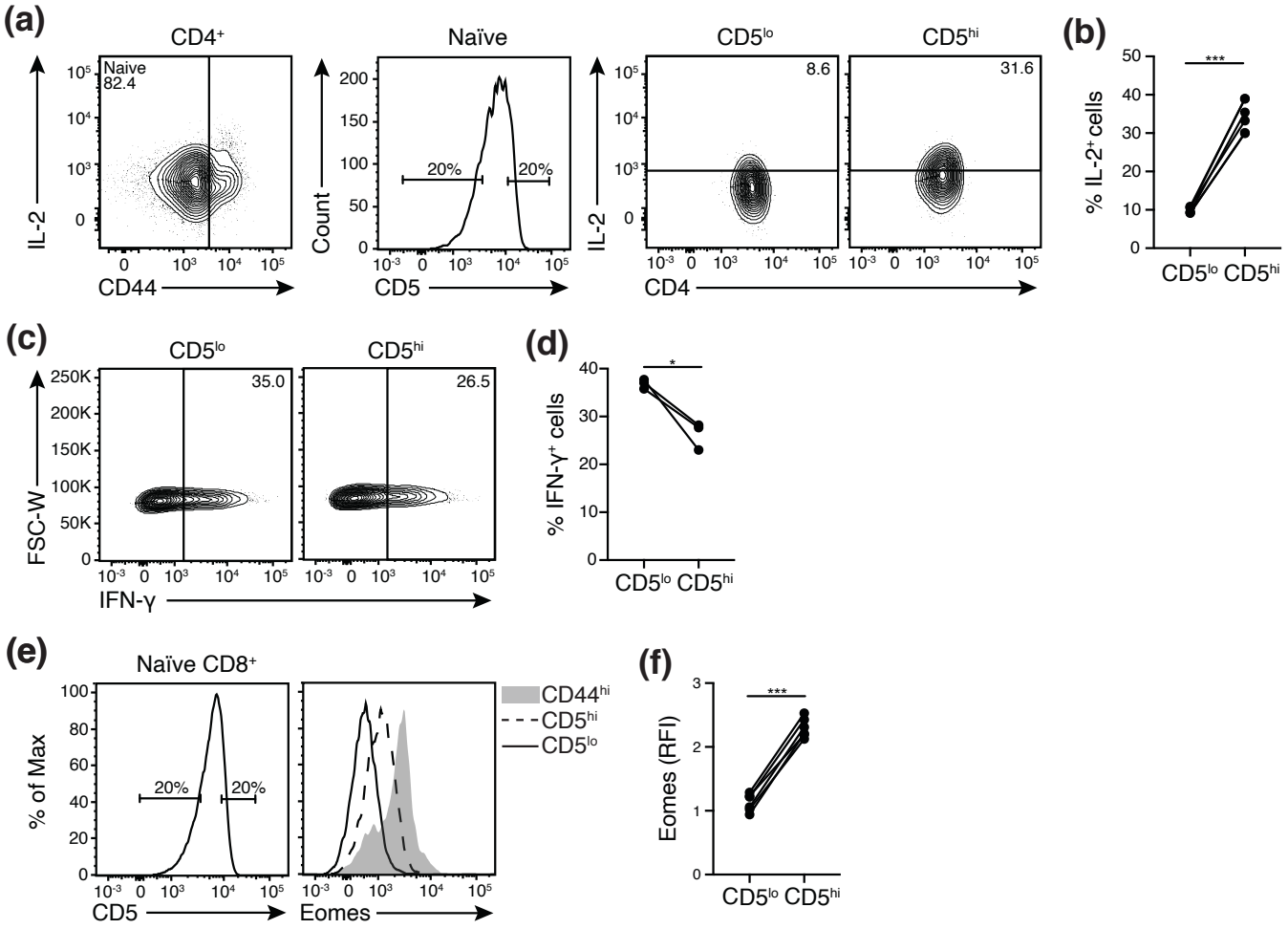
(a)
CD4+
Naive
82.4
IL-2
CD44
Naïve
Count
20%
20%
CD5
CD5lo
CD5hi
8.6
31.6
IL-2
CD4
(b)
% IL-2+ cells
***
CD5lo CD5hi
(c)
CD5lo
CD5hi
35.0
26.5
FSC-W
IFN-γ
(d)
% IFN-γ+ cells
*
CD5lo CD5hi
(e)
Naïve CD8+
% of Max
20%
20%
CD5
Eomes
CD44hi
CD5hi
CD5lo
(f)
Eomes (RFI)
***
CD5lo CD5hi

Supplementary Figure 1

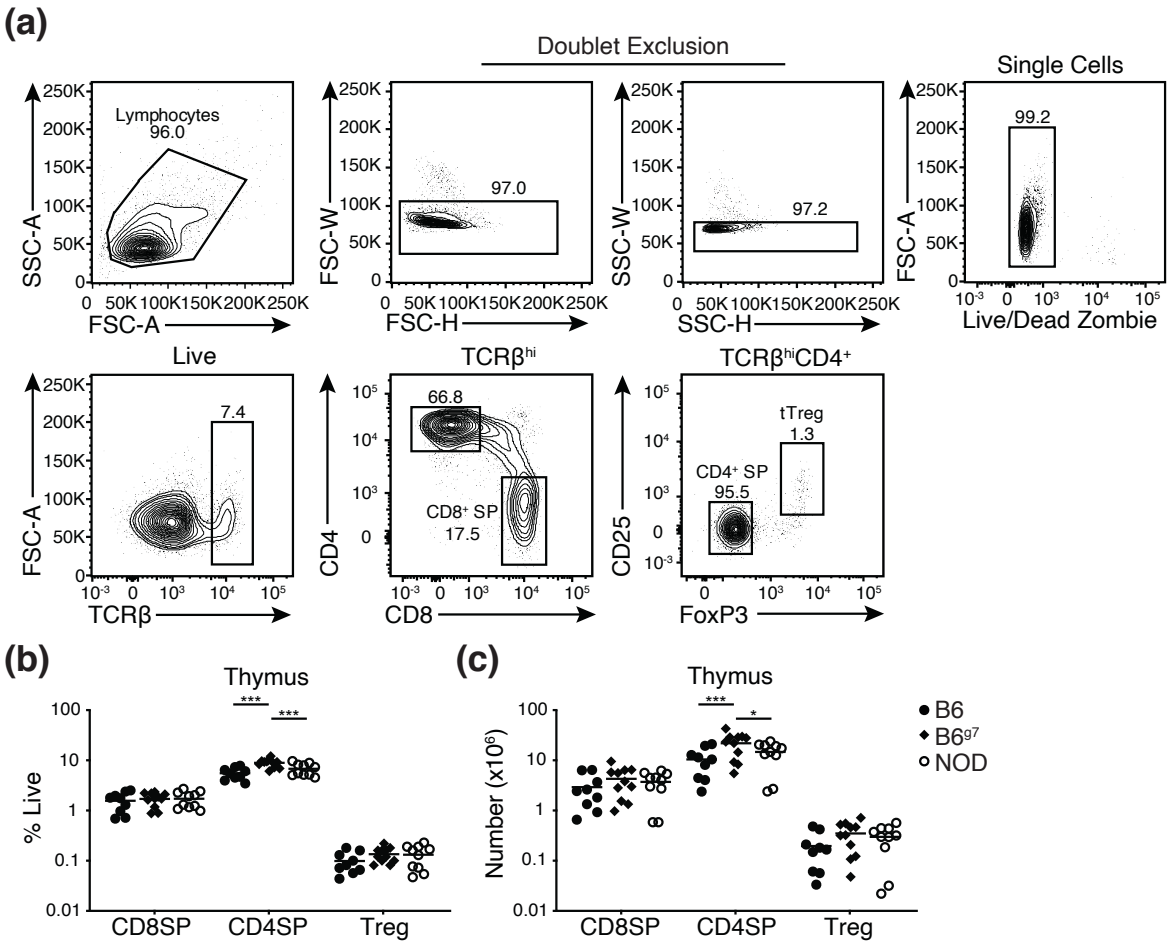

Supplementary Figure 1. Equivalent thymocyte subset proportion and number in B6, B6^{g7}, and NOD mice. **(a)** Representative flow plots depicting gating strategies for CD8$^+$ SP (TCRβ^{hi} CD8$^+$), CD4$^+$ SP (TCRβ^{hi} CD4$^+$CD25$^-$FoxP3$^-$), and thymic Treg (tTreg, TCRβ^{hi} CD4$^+$ CD25$^+$ FoxP3$^+$) B6 thymocytes. **(b)** Percentage and **(c)** absolute numbers of CD8$^+$ SP, CD4$^+$ SP and tTreg thymocyte subsets from B6, B6^{g7}, and NOD mice. Each dot depicts data from an individual mouse from six independent experiments: B6 (n=9), B6^{g7} (n=11), NOD (n=10). One-way ANOVA followed by Sidak's multiple comparison test, * $P < 0.05$, *** $P < 0.001$.

Supplementary Figure 2

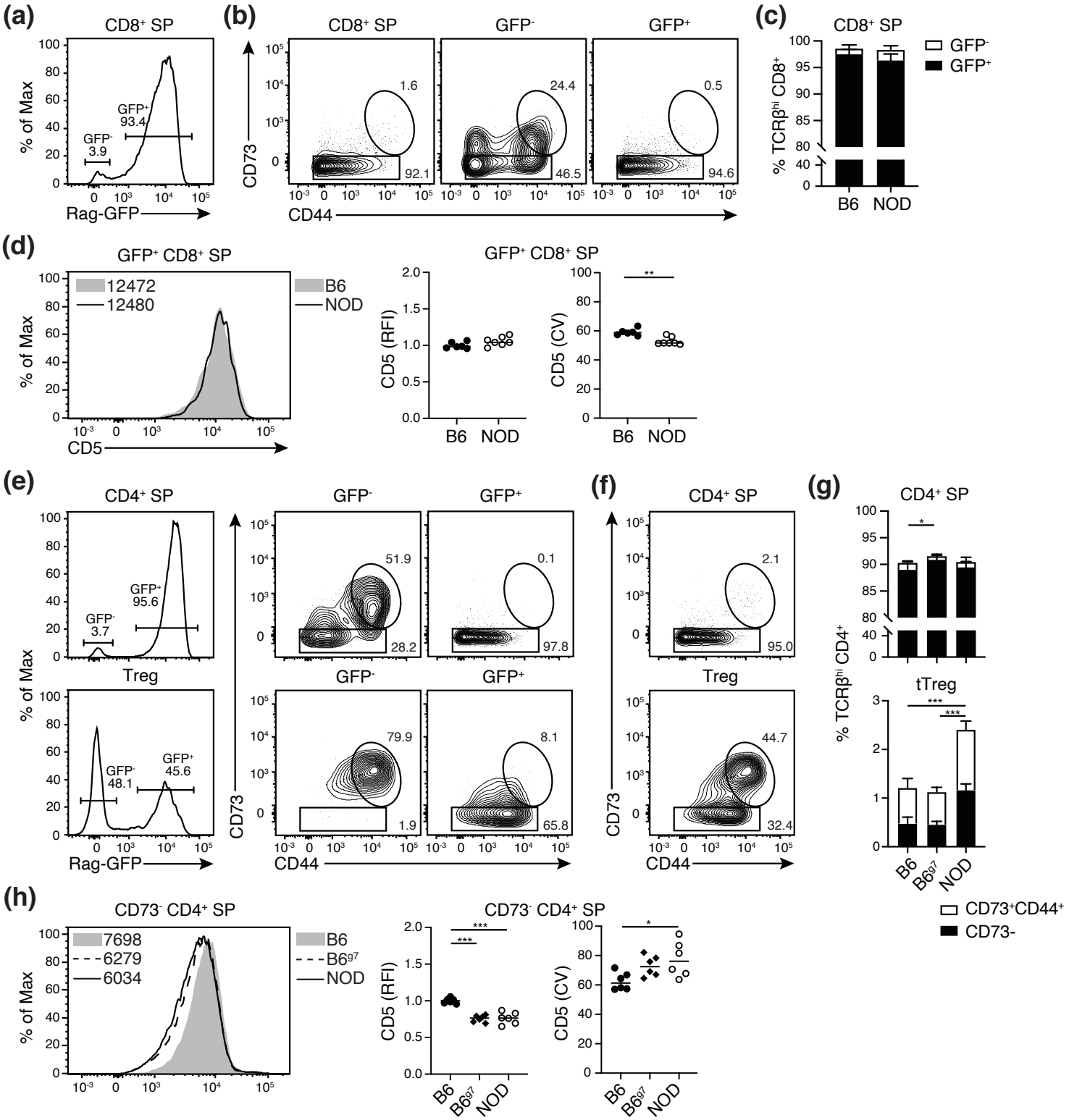

Supplementary Figure 2. Rag2-GFP and CD73 staining to identify T cells recirculating to the thymus. **(a)** Representative histogram for gating GFP$^-$ (recirculating) and GFP$^+$ (non-recirculating) populations on CD8$^+$ SP. **(b)** Representative flow plots for gating CD73$^-$ (non-recirculating) or CD73$^+$CD44$^+$ (recirculating) T cells in total CD8$^+$ SP, GFP$^-$ and GFP$^+$ CD8$^+$ SP. **(c)** Proportion of GFP$^-$ and GFP$^+$ CD8$^+$ SP from B6.Rag-GFP and NOD.Rag-GFP mice. **(d)** Representative histograms of CD5 expression, CD5 relative fluorescent intensity (RFI) and CD5 coefficient of variation (CV) on GFP$^+$ CD8$^+$ SP from B6.Rag-GFP and NOD.Rag-GFP mice. The RFI is calculated by normalizing to the average of the CD5 mean fluorescent intensity MFI on CD8$^+$ SP thymocytes from B6.Rag-GFP mice in each experiment. Each dot depicts data from an individual mouse; B6.Rag-GFP (n=6) and NOD.Rag-GFP (n=7). **(e)** Representative histograms gating GFP$^-$ and GFP$^+$ populations on CD4$^+$ SP and tTregs, and flow plots depicting corresponding GFP$^-$ and GFP$^+$ with and CD73 and CD44 expressions. **(f)** Representative flow plots for CD73 and CD44 expression on total CD4$^+$ SP and tTregs. **(g)** Proportion of CD73$^+$CD44$^+$ and CD73$^-$ CD4$^+$ SP and tTregs from B6, B6^{g7}, and NOD mice. (h) Representative histograms of CD5 expression, CD5 RFI and CD5 CV on CD4$^+$ SP from B6, B6^{g7}, and NOD mice. The RFI is calculated by normalizing to the average of the CD5 MFI on CD4$^+$ SP thymocytes from B6 mice in each experiment. Each dot depicts data from an individual mouse; B6 (n=6), B6^{g7} (n=6), NOD (n=6). The data was obtained in two independent experiments that included at least one mouse per strain. Unpaired two-tailed student *t*-test or one-way ANOVA followed by Sidak's multiple comparison test, * $P < 0.05$, ** $P < 0.01$, *** $P < 0.001$.

Supplementary Figure 3

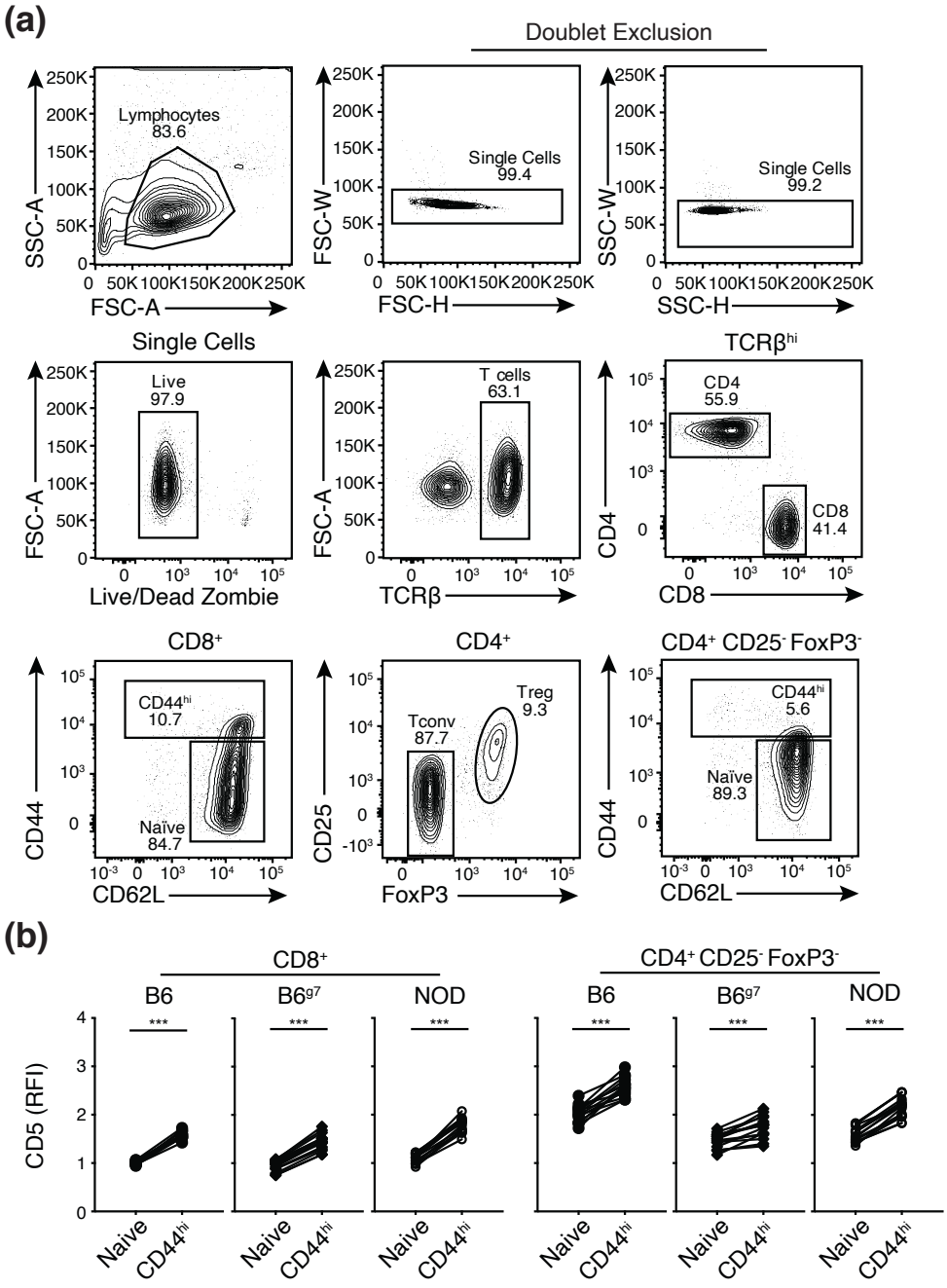

Supplementary Figure 3. CD44^{hi} T cells express higher levels of CD5 than naïve T cells. **(a)** Representative flow plots depicting gating strategies for naïve CD8$^+$ T cells (TCRβ$^+$ CD8$^+$ CD62L$^+$ CD44$^-$) and CD44^{hi} CD8$^+$ T cells (TCRβ$^+$ CD8$^+$ CD44$^+$), then for Tregs (TCRβ$^+$ CD4$^+$ CD25$^+$ FoxP3$^+$) and conventional CD4$^+$ T cells (Tconv, TCRβ$^+$ CD4$^+$ CD25$^-$ FoxP3$^-$). CD4$^+$ T cells are further separated as naïve (CD62L$^+$ CD44$^-$) and CD44^{hi} (CD44$^+$) T cells. **(b)** CD5 RFI on naïve vs CD44^{hi} CD8$^+$ and CD4$^+$ T cells from the peripheral lymph nodes of B6, B6^{g7}, and NOD mice. The RFI was calculated by normalizing to the average of the CD5 MFI on naïve CD8$^+$ T cells from B6 mice in each experiment. Each dot depicts data from an individual mouse from six independent experiments; B6 (n=15), B6^{g7} (n=17), NOD (n=16). One-way ANOVA followed by Sidak's multiple comparison test, *** $P < 0.001$.

Supplementary Figure 4

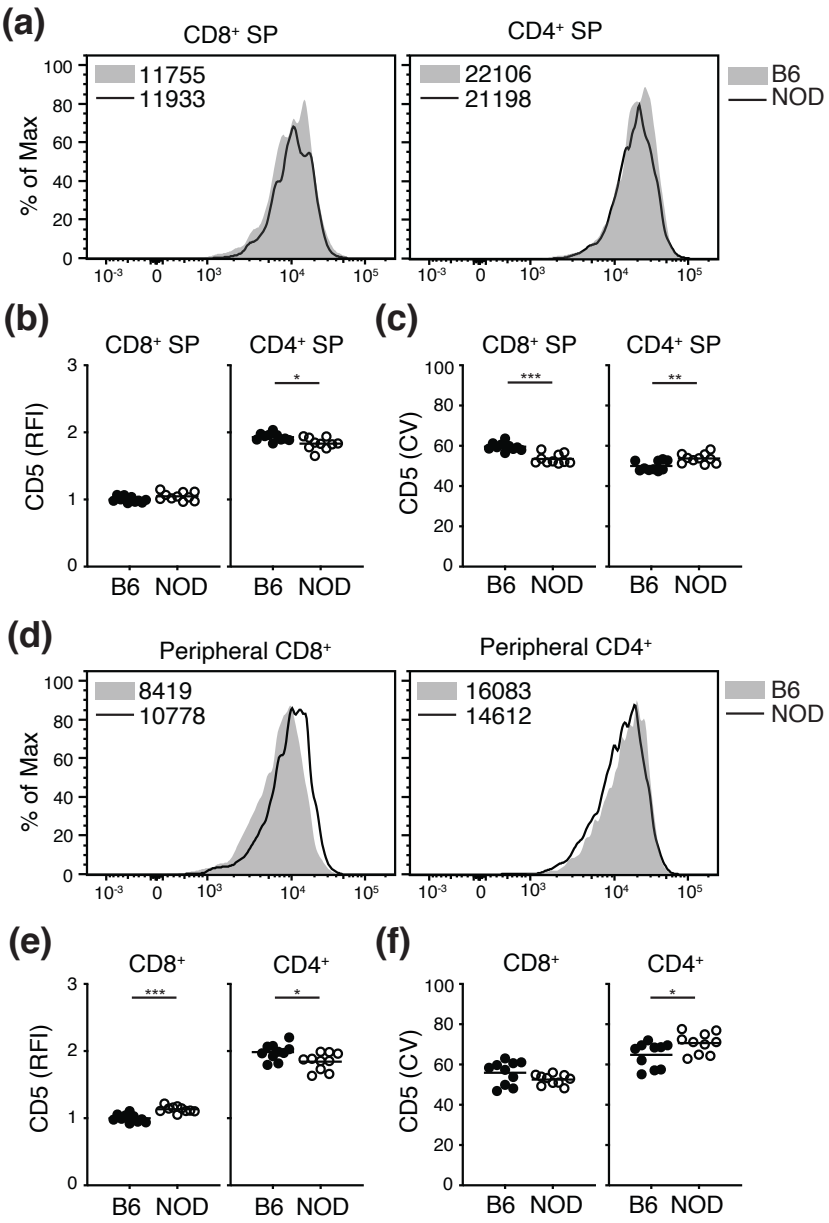

Supplementary Figure 4. Peripheral T cells from NOD mice in a different facility also express differential CD5 levels as compared to their B6 counterparts. **(a)** Representative histograms of CD5 expression on TCRβ^{hi} CD8$^+$ SP and CD4$^+$ SP thymocytes from B6 (grey shaded) and NOD (solid line) mice. **(b)** CD5 RFI and **(c)** CD5 CV on CD8$^+$ SP and CD4$^+$ SP from B6 and NOD mice. **(d)** Representative histograms of CD5 expression on TCRβ^{hi} CD8$^+$ and CD4$^+$ splenic T cells from B6 (grey shaded) and NOD (solid line) mice. **(e)** CD5 RFI and **(f)** CD5 CV on CD8$^+$ and CD4$^+$ splenic T cells from B6 and NOD mice. The RFI is calculated by normalizing to the average of the CD5 MFI on CD8$^+$ SP thymocytes or CD8$^+$ splenic T cells from B6 mice. Each dot depicts data from an individual mouse from two independent experiments; B6 (n=10), NOD (n=10). Unpaired two-tailed student *t*-test, * $P < 0.05$, ** $P < 0.01$, *** $P < 0.001$.

Supplementary Figure 5

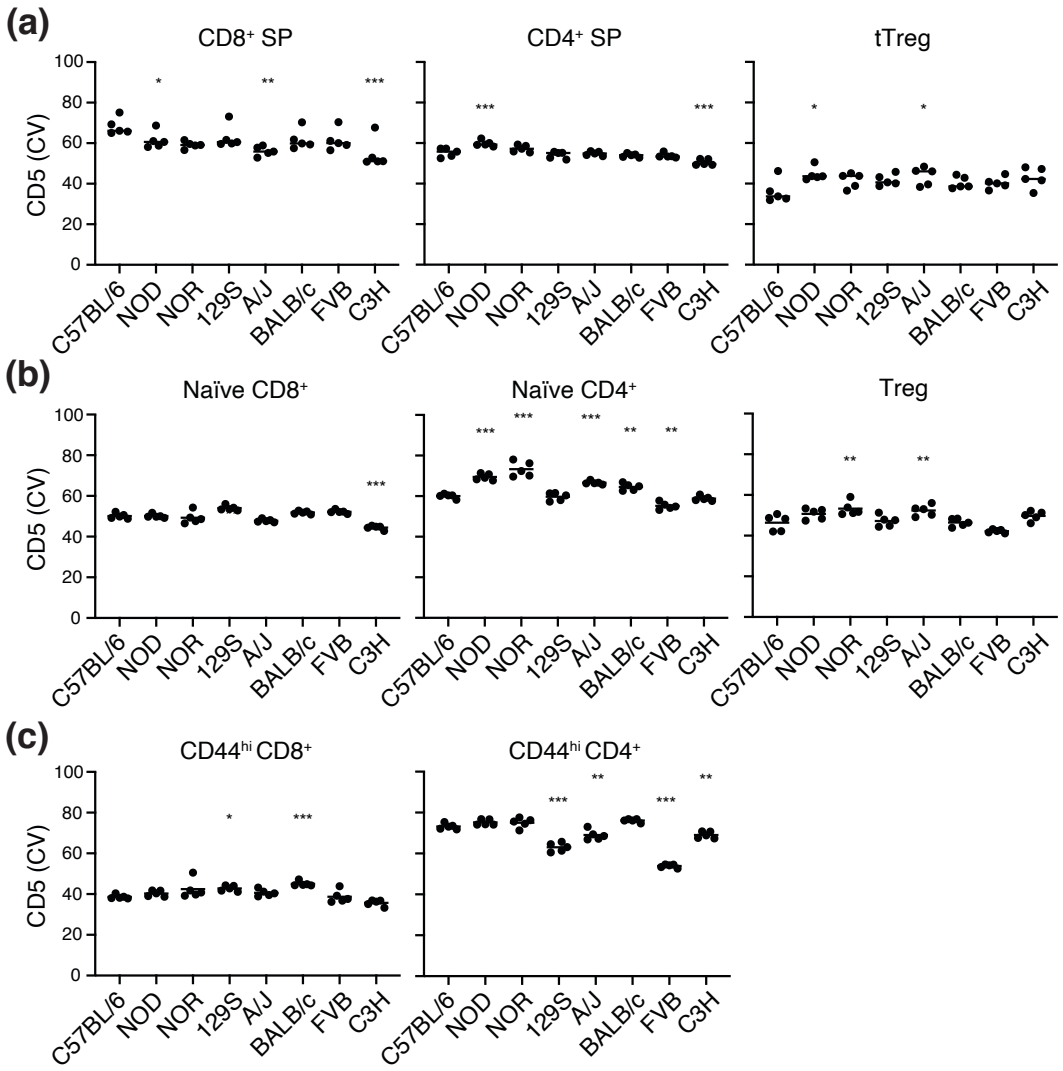

Supplementary Figure 5. CD5 coefficient variations (CV) in eight different mouse strains. CD5 CV on **(a)** $CD8^+$ SP and $CD73^-$ $CD4^+$ SP thymocytes, as well as $CD73^-$ tTregs; **(b)** naïve $CD8^+$, naïve $CD4^+$ and Tregs from the peripheral lymph nodes; and **(c)** $CD44^{hi}$ $CD8^+$ and $CD44^{hi}$ $CD4^+$ from peripheral lymph nodes for indicated mouse strains. The data was obtained in two independent experiments that included at least one mouse per strain; n=5 for each strain. One-way ANOVA followed by Dunnett's multiple comparison test where each strain is compared to C57BL/6, * $P < 0.05$, ** $P < 0.01$, *** $P < 0.001$.

Supplementary Figure 6

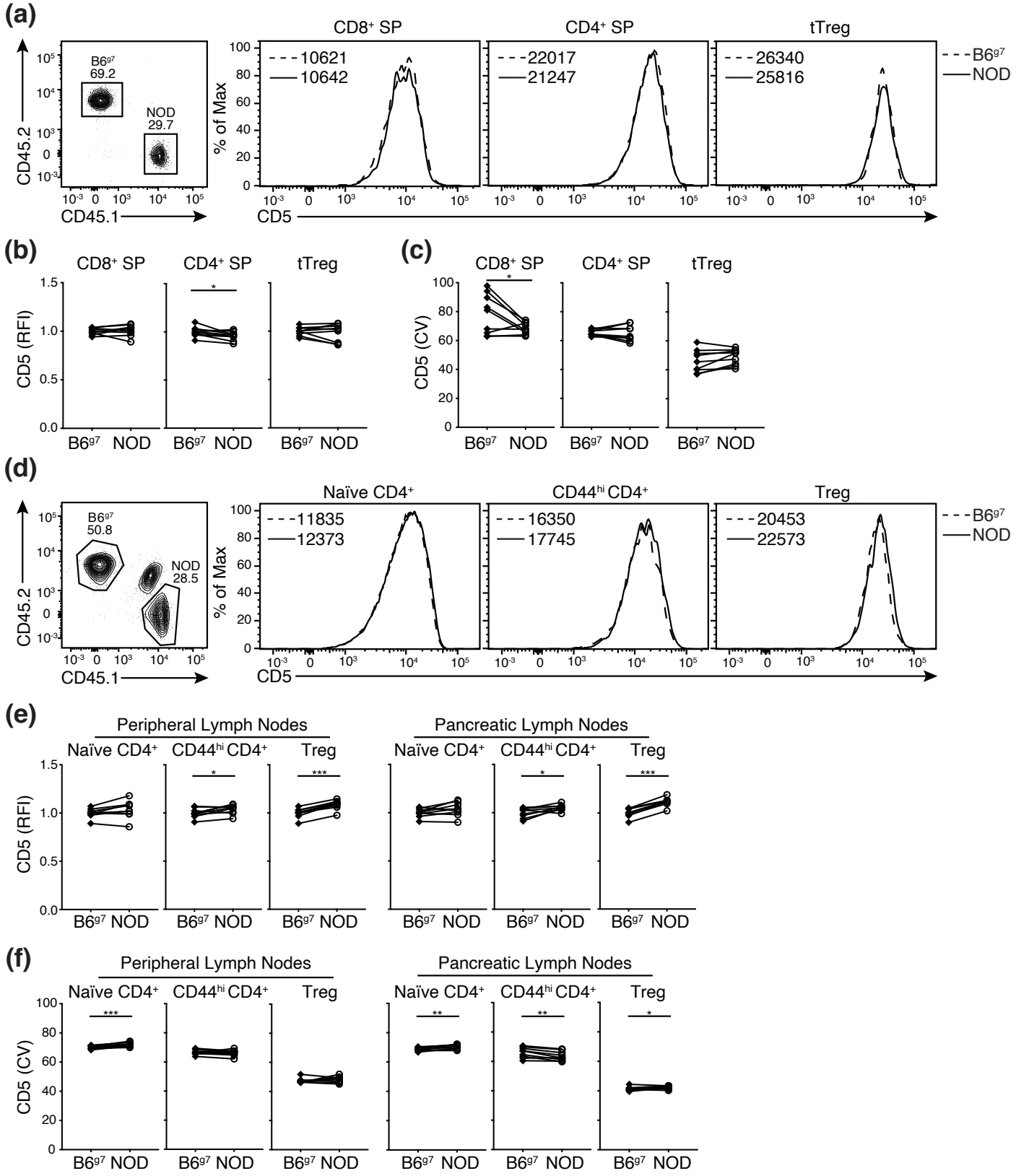

Supplementary Figure 6. Similar CD5 expression on peripheral CD4$^+$ T cells from B6^{g7} and NOD donor cells in bone marrow chimeras. **(a)** Representative flow plot of total thymocytes and histograms of CD5 expression of B6^{g7} and NOD bone-marrow-derived CD8$^+$ SP (TCRβ^{hi} CD8$^+$), CD4$^+$ SP (TCRβ^{hi} CD4$^+$CD25$^-$ FoxP3$^-$), and tTreg (TCRβ^{hi} CD4$^+$CD25$^+$ FoxP3$^+$) in F1^{g7} chimeric mice. **(b)** CD5 RFI and **(c)** CD5 CV on B6^{g7}- and NOD-derived CD8$^+$ SP, CD4$^+$ SP and tTregs from the thymus. **(d)** Representative flow plot of peripheral lymph node and histograms of CD5 expression of B6^{g7} and NOD bone-marrow-derived derived CD4$^+$ naïve T cells (TCRβ$^+$ CD4$^+$CD62L$^+$ CD44$^-$ CD25$^-$ FoxP3$^-$), CD44^{hi} T cells (TCRβ$^+$ CD4$^+$CD44$^+$CD25$^-$ FoxP3$^-$), and Treg (TCRβ$^+$ CD4$^+$ CD25$^+$ FoxP3$^+$) in F1^{g7} chimeric mice. **(e)** CD5 RFI and **(f)** CD5 CV on B6^{g7}- and NOD-derived CD4$^+$ naïve T cells, CD44^{hi} T cells, and Treg from peripheral and pancreatic lymph nodes. The RFI was calculated by normalizing to the average of the CD5 MFI on the B6^{g7}-derived subset in each individual experiment. Each dot indicates data from cells of either B6^{g7} or NOD origin in chimeric mice from two independent experiments; n=9. Paired student *t*-test, * $P < 0.05$, * $P < 0.01$, *** $P < 0.001$.

Supplementary Figure 7

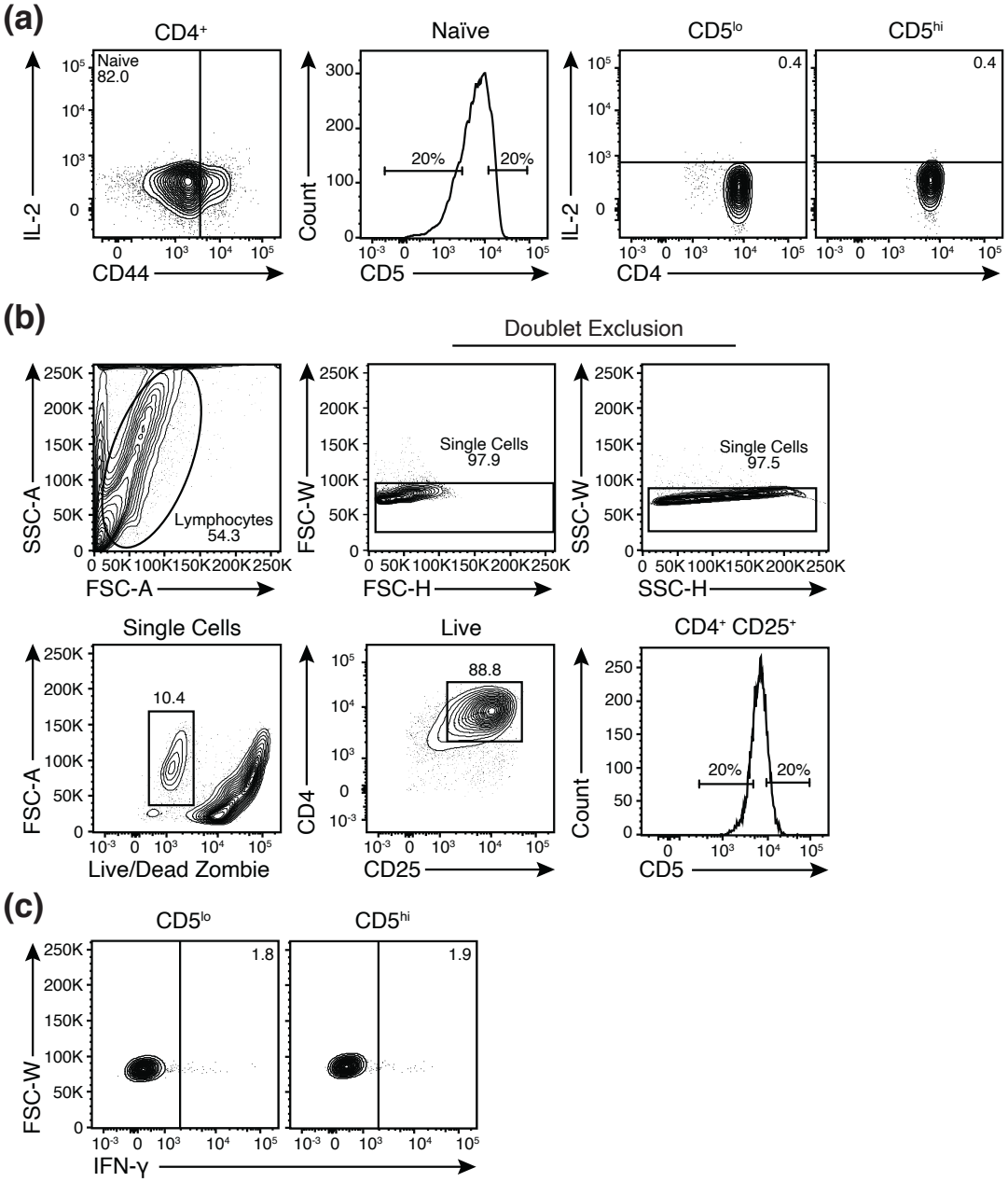

Supplementary Figure 7. Gating strategies for IL-2 and IFN-γ production following PMA-Ionomycin activation and Th1 skewing. **(a)** Representative flow plots depicting the gating strategies for unstimulated controls in PMA-Ionomycin activation experiments. TCRβ+ CD4+ T cells with low expression of CD44 (naïve CD4+) were selected based on the top and bottom 20% of CD5 expression to examine IL-2 production. This gating strategy was applied for PMA-Ionomycin activated samples in Figure 4a. **(b)** Representative gating strategy for enriched naïve CD4+ T cells activated under Th0 or Th1 skewing conditions. **(c)** Minimal IFN-γ production is observed in Th0 control samples.